

Plasmon-Exciton-Polariton Lasing

Mohammad Ramezani,^{1,*} Alexei Halpin,^{1,*} Antonio I.

Fernández-Domínguez,² Johannes Feist,² Said Rahimzadeh-Kalaleh

Rodríguez,³ Francisco J. Garcia-Vidal,^{2,4,†} and Jaime Gómez-Rivas^{1,5,‡}

¹*FOM Institute DIFFER, P.O. Box 6336, 5600 HH Eindhoven, Netherlands*

²*Departamento de Física Teórica de la Materia Condensada*

and Condensed Matter Physics Center (IFIMAC),

Universidad Autónoma de Madrid, E-28049 Madrid, Spain

³*Laboratoire de Photonique et Nanostructures,*

LPN/CNRS, Route de Nozay, 91460 Marcoussis, France

⁴*Donostia International Physics Center (DIPC),*

E-20018 Donostia/San Sebastian, Spain

⁵*COBRA Research Institute, Eindhoven University of Technology,*

P.O.Box 513, 5600 MB Eindhoven, The Netherlands

(Dated: March 29, 2022)

arXiv:1606.06866v1 [cond-mat.mes-hall] 22 Jun 2016

* These two authors contributed equally

† fj.garcia@uam.es

‡ j.gomezrivas@diffier.nl

Strong coupling of Frenkel excitons with surface plasmons leads to the formation of bosonic quasi-particles known as plasmon-exciton-polaritons (PEPs). Localized surface plasmons in nanoparticles are lossy due to radiative and non-radiative decays, which has hampered the realization of polariton lasing in a plasmonic system, i.e., PEP lasing. These losses can be reduced in collective plasmonic resonances supported by arrays of nanoparticles. Here we demonstrate PEP lasing in arrays of silver nanoparticles by showing the emergence of a threshold in the photoluminescence accompanied by both a superlinear increase of the emission and spectral narrowing. We also observe a reduction of the threshold by increasing the coupling between the molecular excitons and the resonances supported by the array despite the reduction of the quantum efficiency of the emitters. The coexistence of bright and dark collective modes in this plasmonic system allows for a 90° -change of polarization in the emission beyond the threshold.

Strong light-matter interaction and the resulting formation of exciton-polaritons has been a major field of scientific research over the past two decades [1]. Particularly in the realm of semiconductor microcavities, several fascinating phenomena including parametric processes [2, 3], Bose-Einstein condensation (BEC) [4] and superfluidity [5] have all been shown to emerge through the interactions of exciton-polaritons with each other and their environment.

Recent reports have extended exciton-polariton studies to room-temperature organic systems [6–10], where several independent studies have reported polariton lasing/BEC [11, 12] and shown nonlinear interactions in the condensate [13]. Organic systems are generally disordered but have strong transition dipole moments, allowing them to couple efficiently to the electromagnetic field despite their broad linewidths and strong vibronic coupling. Sufficiently strong-light matter coupling has already been shown to mitigate those effects leading to novel behaviours, such as enhanced exciton transport and conductivity [14–16], in addition to the modification of molecular structures and chemical reactions [17, 18].

In this aim, microcavities have provided a robust platform for experimentation, as they support low loss photonic modes with high quality factors (and thus narrow linewidths), which can be easily tuned to excitonic resonances. Another strategy for achieving strong coupling has focused on using strong scatterers such as plasmonic systems, where particles with subwavelength dimensions can strongly enhance the electric field intensity in their vicinity. Indeed, in spite of the significantly lower quality factor of the plasmonic resonances relative to their counterparts in dielectric microcavities, strong coupling has been observed in several plasmonic systems [8, 10, 19–24], suggesting new cavity architecture designs to investigate the nonlinear behaviour of hybridized quasi-particles. However, lasing of PEPs has not been observed so far, most likely because of the large losses associated with localized surface plasmon (LSP) resonances.

Here we take advantage of a special type of plasmonic modes that are supported by periodic arrays of metal nanoparticles, the so-called surface lattice resonances (SLRs). These modes are the result of the enhanced radiative coupling between LSP resonances with Rayleigh Anomalies (RAs), i.e., in-plane orders of diffraction in the periodic structure. Energy dispersions and quality factors of these SLRs can be tailored by varying the geometrical parameters and energy detuning between RAs and LSP resonances [25, 26]. In addition, the enhanced in-plane radiative coupling reduces the radiative losses associated to localized resonances [2] and the redistribution of the electromagnetic field around the particles also

reduces Ohmic losses [28], creating narrow resonances with high quality factors [2, 4, 29]. Therefore, SLRs are ideal candidates to become the plasmonic component of hybrid PEPs for lasing.

We first demonstrate strong-coupling between excitons in an organic dye and the SLRs supported by an array of silver nanoparticles leading to the formation of PEPs. Subsequently, at very high PEP densities, we observe the appearance of stimulated scattering and PEP lasing. Previous implementations of photon lasing from plasmonic systems have focused on the weak coupling regime with efficient emitters, where stimulated emission occurs via surface plasmons [31, 32] or where the surface plasmons contribute to increasing gain, both via resonant energy transfer [34, 35] and modification of modal dispersions in distributed feedback (DFB) configurations [36]. In addition, earlier attempts toward achieving PEP lasing remained unsuccessful due to the inefficient relaxation mechanism of PEPs and the saturation of strong coupling at large pumping fluences [21]. In the measurements below we investigate an entirely different regime, where despite quenching in the emission due to the very high concentration of molecules, we observe a threshold for non-linear emission at high densities of PEPs. This nonlinear emission or PEP lasing occurs when stimulated scattering provides a mean to condense these PEPs into a low momentum state, from which emission proceeds.

In Fig. 1 we show the normalized absorption and photoluminescence (PL) spectra of a layer of PMMA doped with organic dye molecules. We use a rylene dye [N,N'-Bis(2,6-diisopropylphenyl)-1,7- and -1,6-bis(2,6-diisopropylphenoxy)-perylene-3,4:9,10-tetracarboximide] as an emitter [37], due to its high photostability and low propensity towards aggregation at high concentrations. Two distinct peaks corresponding to the main electronic transition at $E = 2.24$ eV and first vibronic sideband at $E = 2.41$ eV are evident in the absorption spectra of the molecules. A layer of PMMA doped with dye molecules with thickness of 260 nm is spin-coated on top of the plasmonic array of silver nanoparticles. A SEM image of the fabricated array is depicted in the inset of Fig. 1. The array consists of particles with dimensions of $200 \times 70 \times 20$ nm³ and the pitch sizes along the x and y directions are 200 nm and 380 nm, respectively.

First, we measure the angle-resolved extinction of the nanoparticle array when covered by an undoped layer of PMMA (Figs. 2(a,c)). The polarization of the incident light is fixed, and set to be either perpendicular (top row) or parallel (bottom row) to the long axis of the

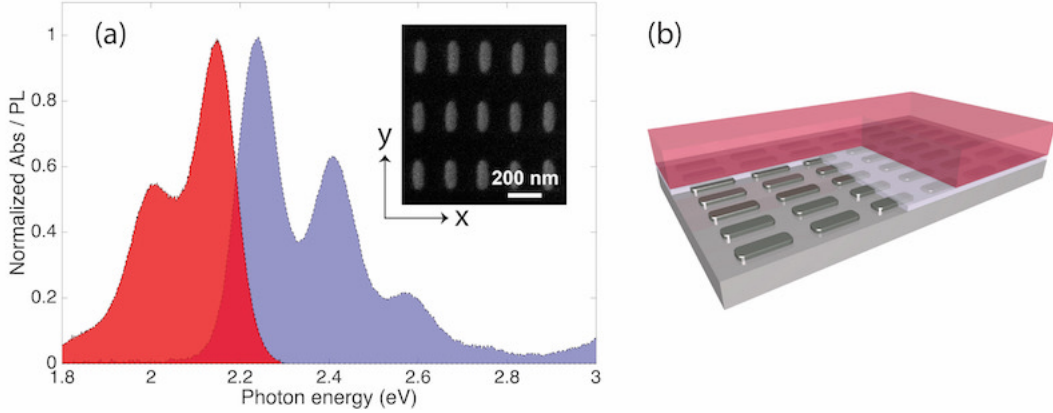


FIG. 1. (a) Normalized absorption (blue) and PL (red) spectra of the layer of PMMA doped with dye molecules in the absence of the plasmonic array. The inset shows an SEM image of the array of silver nanoparticles. (b) Schematic illustration of the array covered with a thin layer of PMMA doped with dye molecules.

nanoparticles as indicated by the arrow in the inset. By probing the sample under different polarizations and angles of incidence, we couple to different resonances with distinct electric field distributions and symmetries depending on which RAs are probed. The resonance with parabolic dispersion in Fig. 2(a) demonstrates the combination of both strong extinction and narrow linewidth in SLRs, which results in this case from the enhanced radiative coupling of $(0, \pm 1)$ RAs to a dipolar LSP resonance supported by the individual nanoparticles (see below). Similarly, by rotating the polarizer and aligning the incident electric field along the long axis of the nanoparticles, we probe the coupling of $(0, \pm 1)$ RAs to a quadrupolar LSP resonance supported by the rods (see also below) [5]. Differences between the extinction measurements of Figs. 2(a,c) can be observed, where the most important is the vanishing SLR at $k_{\parallel} = 0$ for the situation in which the incident electric field is polarized along the long axis of the rods. For this case the electric field distribution is not dipole-active along the polarization direction. As a result, coupling of the free space radiation into this mode is inefficient and the mode is dark at normal incidence. This behaviour implies a strong reduction of radiation losses of this mode which, as we will show later, is a key ingredient to achieve PEP lasing [39, 40].

Extinction measurements of the same array in the presence of a 260 nm thick PMMA layer doped with dye molecules are shown in Figs. 2(b,d). The dye concentration (C) in

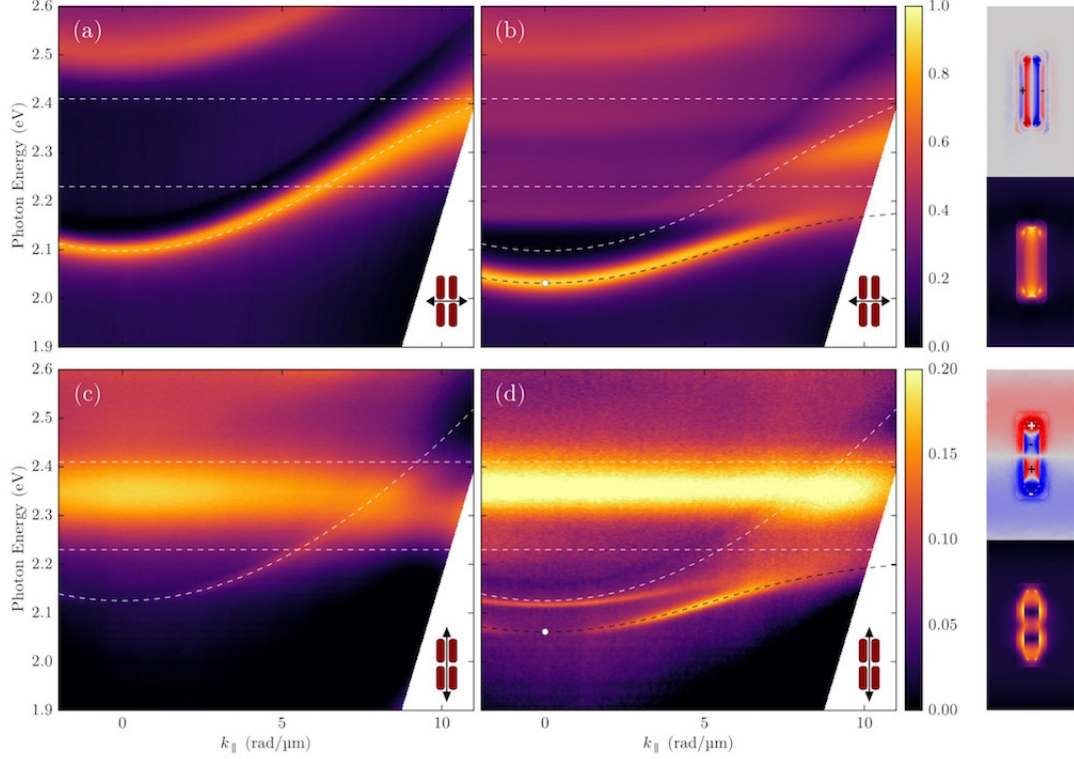


FIG. 2. The extinction measurements of the sample with incident light polarized along the short axis of the nanoparticles in the absence (a) and the presence (b) of the dye molecules. The extinction of the same sample illuminated by the light polarized along the long axis of the nanoparticles without (c) and with (d) the dye. The white dashed lines indicate the energies of the two strongest vibronic transitions in the molecules (horizontal lines) and the SLR dispersion whereas the dashed black lines correspond to the lowest PEP modes. Right panels: maps of the electric field amplitude and induced charge density for the corresponding lowest PEP modes at $k_{\parallel} = 0$.

the polymer is 35 wt% and the measurements are referenced to the extinction of the doped layer without the nanoparticles. For both polarizations we observe an anticrossing in the extinction dispersion and an associated Rabi splitting, $\hbar\Omega = 200$ meV, at $k_{\parallel} \approx 7$ mrad/nm, which is a fingerprint of the emergence of strong coupling between the SLR and molecular excitations. The coupling leads to the creation of upper and lower PEPs where hybridization occurs for both bright and dark modes. In Fig. 2(d), another resonance slightly blue shifted from the lower PEPs is visible. This resonance corresponds to the guided-mode supported by the polymer layer. The appearance of this guided mode is due to the increase of the

refractive index of the doped polymer layer when the molecular concentration is increased.

In order to analyze the hybrid light-matter nature of the PEPs formed by strong coupling of the SLRs to the dye molecules, we use a few-level Hamiltonian that reproduces the measured dispersions in the extinction and allows the determination of the Hopfield coefficients defining the exciton and photon components of the strongly coupled system. We treat each field polarization separately, with Hamiltonian (for each in-plane momentum)

$$H = \begin{pmatrix} E_{SLR} & g_1 & g_2 \\ g_1 & E_{dye,1} & 0 \\ g_2 & 0 & E_{dye,2} \end{pmatrix}, \quad (1)$$

where E_{SLR} is the energy of the SLR, $E_{dye,1}$ ($E_{dye,2}$) is the energy of the first (second) absorption peak of the dye, and g_1 (g_2) describes the coupling between the SLR and the molecular modes. In Fig. 2, both the input energies of the “bare” states and the energy of the lowest PEP modes are depicted. As the actual system contains additional states at higher energies that we do not treat, we only show the lowest coupled state in the figure. From this analysis we can extract the Hopfield coefficients of the lower PEP. This analysis indicates that the PEP at $k_{\parallel} = 0$ is composed of about 75% SLR and 25% molecular excitations, with similar values obtained for both polarizations. We note here that while the SLR for the polarization along the long axis of the particles is dark under far-field excitation at $k_{\parallel} = 0$, the coupling to the molecules occurs in the near field and thus attains similar strengths for both polarizations.

Electromagnetic calculations were also performed to simulate the extinction properties of the experimental samples. Both FDTD (LumericalTM) and FEM (Comsol MultiphysicsTM) methods were employed, finding an excellent agreement with the extinction maps in Fig. 2 (see Supplementary Information for details). Geometric and material parameters were extracted from SEM images of the samples and previous literature [1], respectively. The right insets in Fig. 2, render electric field amplitude and induced surface charge density maps evaluated at $k_{\parallel} = 0$. The top insets show that, for a polarization along the short axis, the near-field is governed by the bright dipolar ($\lambda/2$) LSP supported by the rods, as anticipated above. On the contrary, the bottom insets indicate that a dark quadrupolar LSP ($3\lambda/2$) resonates for incoming light polarized along the long axis of the rod. Importantly for lasing purposes, both polaritonic modes spectrally overlap within an energy window of

a few meV.

The vacuum Rabi frequency defining the coupling strength is given by $\Omega \propto \sqrt{N}$, where N is the number of excitons within the mode volume of the resonance. Therefore, achieving strong coupling with organic molecules requires increasing their concentration within the polymer matrix such that the exciton density is maximized [20, 22, 35]. However, one immediate drawback of increasing concentration for the emission is caused by interactions between dye molecules at high concentrations, which can lead to spontaneous aggregation (modifying the spectral properties of the sample) and also to a reduction of fluorescence lifetime (τ) due to the enhancement of non-radiative decay channels (concentration quenching of the emission) [42]. Importantly, the dye molecules used here do not suffer from aggregation at high concentrations. To quantify the concentration quenching, we have measured the lifetime and quantum efficiency of the polymer layers with different concentrations (see Supplementary Information for details). One can see that at low concentrations the quantum efficiency of the molecules is close to the unity and the lifetime of the excited molecules is 5.8 ns. However, by increasing the concentrations to 35 wt% the quantum efficiency is reduced to 3 % with the corresponding lifetime of 400 ps. The emissive properties of high concentration samples are thus unsuitable for stimulated emission and photon lasing, where a high quantum yield is desired for achieving gain. In fact, the prediction that lasing without inversion could be achieved by exploiting many-body coherence in strongly coupled exciton-photon systems was a major motivation for the development of exciton-polariton lasers [43].

In order to investigate PEP lasing, we optically pump the sample nonresonantly and measure the PL spectra as a function of the incident excitation power for different concentration of the molecules. The wavelength of the pump laser is centered at $\lambda_{exc} = 500$ nm ($E_{exc} = 2.48$ eV) and the pump polarization is fixed along the short axis of the nanoparticles for all experiments. The spectra of the PL for the sample with C= 35 wt% in the forward direction for different absorbed pump fluences is shown in Fig. 3(a), where we observe the appearance of a very sharp peak in the emission spectrum at a fluence of $18 \mu\text{J}/\text{cm}^2$. In Fig. 3(b), we plot the maximum of the PL intensity as a function of absorbed pump fluence for three different concentrations of dye. For the low concentration sample, C = 15 wt%, the PL intensity increases linearly with the incident power. This sample is at the onset of the appearance of exciton-SLR hybridization in extinction (see Supplementary Information). At

$C = 25$ wt%, we observe the emergence of a threshold in the PL, followed by a superlinear increase of the emission. The nonlinear response of the system is further increased at $C = 35$ wt% where the threshold fluence is lowered by a factor of 2. The linewidth of the PL as a function of the absorbed pump fluence is shown in Fig. 3(c), where a strong reduction of the linewidth above threshold and hence, substantial increase of the temporal coherence, can be observed. In Fig. 3(d) we display the polarization of the emission below and above the threshold for the sample with $C = 35$ wt%. Below the threshold, the emission of the sample is mainly polarized along the short axis of the particles, i.e., 90° . This emission is associated with PEPs originating from the hybridization of the bright SLR with excitons (see Fig. 2(b)). Interestingly, above the threshold, the polarization of the emission rotates by 90° and is primarily oriented along the long axis of the particles. This polarization rotation strongly indicates that the emission above threshold is dominated by the PEPs created from the dark modes whose polarization point to the long axis of the particles (see Fig. 2(d)).

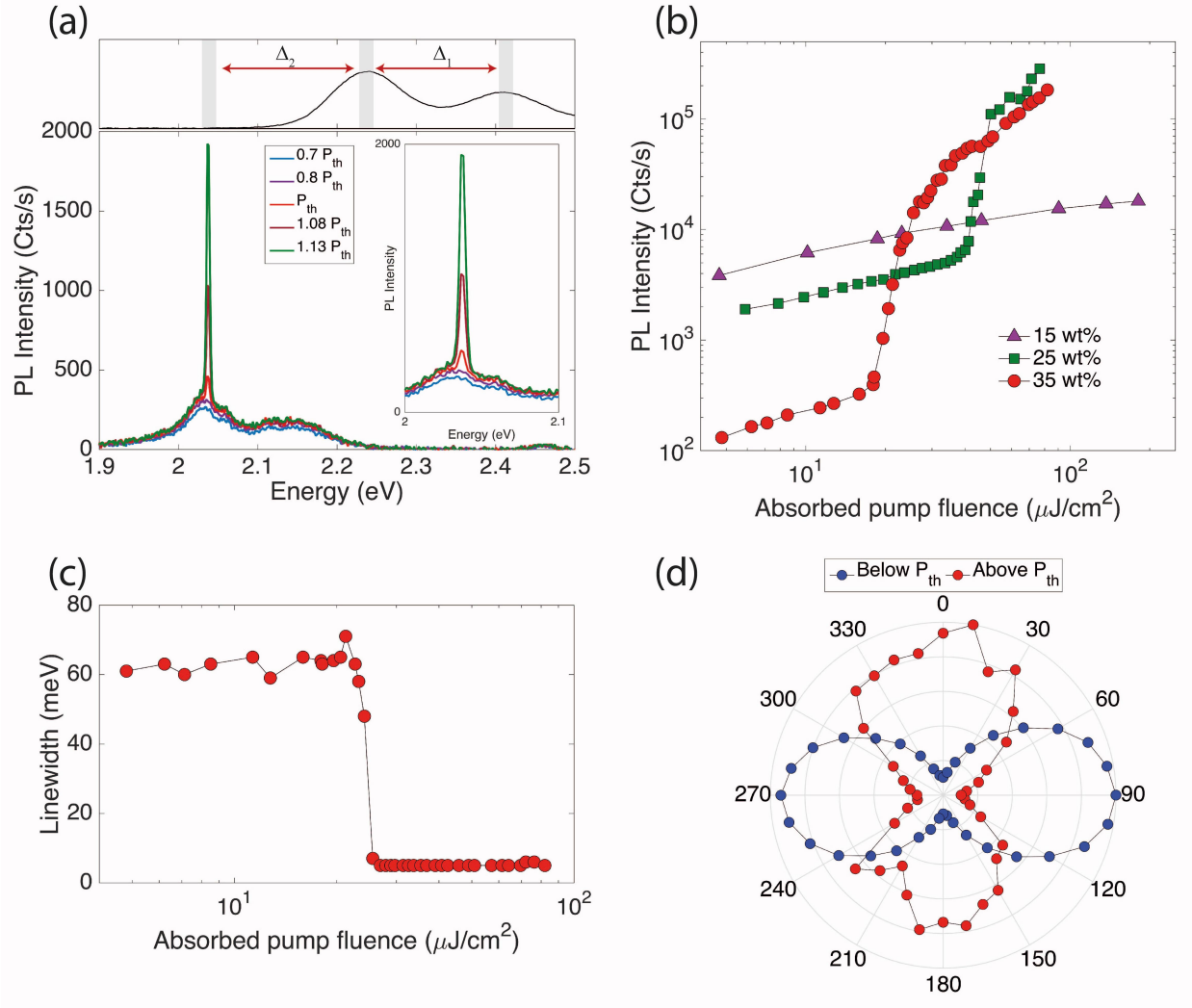


FIG. 3. (a) Emission spectra along the forward direction for the array of nanoparticles covered with PMMA with the dye concentration of 35 wt % at increasing absorbed pump fluences. (Inset) Close view of the lasing peak. Upper panel: Absorption spectrum of the dye (solid curve). The energies of the lasing emission, the main electronic transition and the first vibronic side band of the molecule are indicated by the blue shaded areas. Note that the energy differences Δ_1 and Δ_2 are equal. (b) Photoluminescence peak intensity as a function of absorbed pump fluence for three samples at different concentrations. (c) Linewidth of the photoluminescence peak as a function of absorbed pump energy for the sample with C= 35 wt% dye concentration. (d) Polarization of the emission from the sample with C= 35 wt% below and above threshold ($P = 1.5P_{th}$). The long axis of the nanoparticles is oriented along the vertical direction ($\theta = 0^\circ$).

After excitation the molecules relax to the PEP band. In this incoherent relaxation, the

in-plane momentum is not conserved, leading to a broad distribution of excitation across the whole band. Most of the excitation thus ends up in high- k_{\parallel} *reservoir* modes that are almost uncoupled from the SLR [4]. In order to achieve polariton lasing, the population of a single state has to become large enough to obtain significant bosonic stimulation. In semiconductor microcavities, the necessary relaxation from the reservoir typically relies on exciton-polariton and polariton-polariton scattering. In contrast, microscopic models for organic polariton lasing have suggested that vibronic coupling can play a more important role for dissipating excess momentum than exciton-polariton and polariton-polariton scattering [44–46]. In this picture, high frequency intramolecular vibrational modes allow exciton-polaritons to scatter directly from the reservoir towards the lower energy levels [47]. This implies that organic exciton-polariton lasing is most efficient when the relaxation from the reservoir to the lasing state is resonant with a strong optical phonon line [11]. As shown in the top inset of Fig. 3a, this condition is exactly fulfilled in the current setup: the energy difference, Δ , between the vibronic subpeaks of the molecule (the phonon energy) corresponds exactly to the energy difference between the lowest peak and the lasing state. The specific energy at which the polariton lasing occurs also poses an interesting question: while energy shifts are seen as the smoking-gun for interactions between polaritons in semiconductors microcavities, the reported spectral behaviour of polariton lasers in organic systems has been variable [11–13]. Within the excitation levels afforded to us by the laser system, we do not observe appreciable spectral shifts even at very high excitation levels, reinforcing our claim that polariton-polariton interactions play a negligible role in this system and that vibronic coupling is the main responsible for the relaxation process.

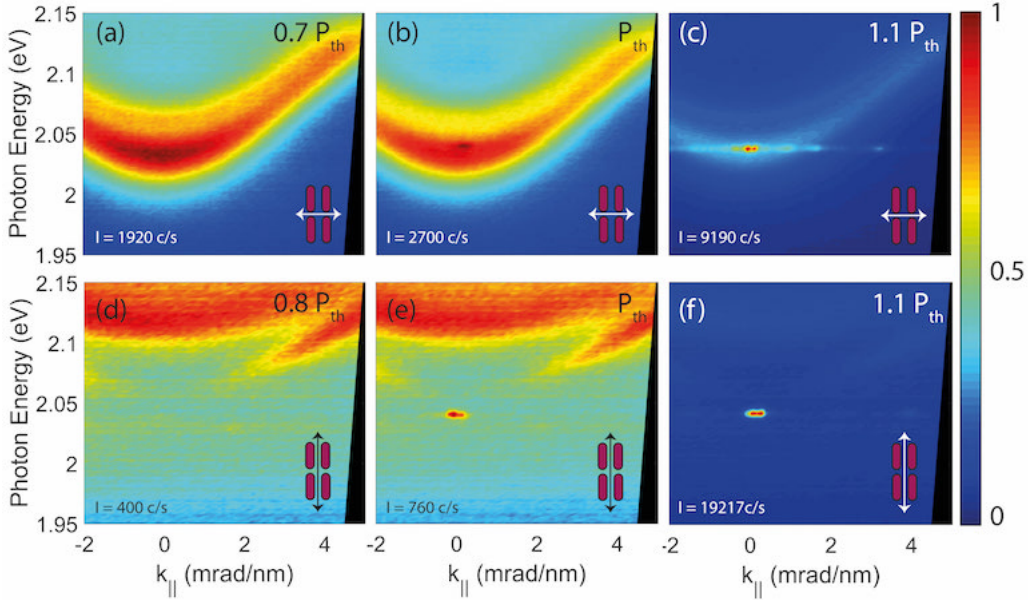


FIG. 4. Normalized angular-resolved emission measurements for two detection polarizations, parallel and orthogonal to the long axis of the nanoparticles, for the array of nanoparticles covered with PMMA with the dye concentration of 35 wt %. The cartoon in the inset of each panel depicts the orientation of the nanoparticles with an arrow indicating the direction of the transmission axis of the polarization analyzer. The emission intensity in unit of counts/s at $E = 2.04$ eV and $k_{\parallel} = 0$ mrad/nm for each detection condition is indicated at the bottom of each panel. (a-c) Angle-resolved PL for different pump fluences with the analyzer along the short axis of the nanoparticle visualizing to the bright mode along $(0, \pm 1)$ RAs supported by the array. (d-f) Angle-resolved PL for different pump fluences with analyzer along the long axis of the nanoparticle. In this configuration, the dark mode excited by $(0, \pm 1)$ RAs is probed.

Similarly to the extinction measurements shown earlier, we can use angular-resolved measurements to study PEP emission at increasing pump fluences as we approach the critical density of PEPs [21]. In Fig. 4, we display the measured dispersion of the emission both below and above threshold for two orthogonal detection polarizations corresponding to the bright and dark modes seen in Figs. 2(b,d). In Figs. 4(a,d), where the pump fluence is below threshold, we recover the same dispersions as those shown previously in the extinction measurements with a bright mode for horizontal polarization and a dark mode for vertical.

We observe emission over the whole range of k_{\parallel} indicating that, as mentioned above, the molecular relaxation process populating the PEPs after high-frequency excitation does not conserve $k_{\parallel} = 0$. Upon increasing the pump fluence, we observe a collapse in the emission pattern towards $k_{\parallel} = 0$ over the narrow spectral range seen in the spectra of Fig. 3(a). As we mentioned earlier, while the system exhibited no vertically polarized emission at normal incidence below threshold, above threshold the lasing peak is mainly polarized along this direction. This behaviour highlights one of the major differences between open systems defined by plasmonic lattices and traditional microcavities: the bright mode corresponding to the SLR of Fig. 2(a) represents a lossy mode due to the radiation losses as it can efficiently couple out into free-space. On the other hand, the dark-mode is significantly less lossy at $k_{\parallel} = 0$ due to suppression of radiation losses, which favors PEP lasing at this mode. The PEPs created via this mode can be accumulated with a much lower probability of decay.

In conclusion, we have demonstrated the first exciton-polariton laser from a plasmonic-based open cavity. Using a nanoparticle array which supports spectrally sharp modes, we achieve strong coupling to the electronic transitions of molecules in a highly doped polymer layer. The array supports both bright and dark electromagnetic modes, which provide channels with different loss rate, in which polaritons can accumulate leading to PEP lasing. Since the array properties can be easily tuned, by varying the excitonic content of the PEPs, it should be possible to exert further control over the emission properties. These experiments reveal the feasibility of achieving bosonic stimulated scattering processes in the proximity of lossy plasmonic systems in an open and planar structure, and provide an example of how plasmonic systems are very well suited for investigating nonequilibrium physics of exciton-polaritons.

METHODS

Fabrication

The array of silver nanoparticles was fabricated by substrate conformal nanoimprint lithography following the procedure described in Ref.[48] on glass (Eagle 2000) and encapsulated by 8 nm of SiO₂ and 20 nm of Si₃N₄ to prevent oxidation of silver.

Characterization

The extinction measurements have been performed using a collimated polarized white light beam generated from a halogen lamp. The zeroth-order transmission of the white light from the sample under different incident angles ($T_0(\theta)$) is collected. For the reference measurement, the transmitted light through the same substrate and the polymer layer in the absence of the array ($T_0^{ref}(\theta)$) is measured. The extinction is defined as $1 - T_0(\theta)/T_0^{ref}(\theta)$.

The photoluminescence measurements have been done with amplified pulses generated from an optically parametric amplifier with an approximate pulse duration of 100 fs and a repetition rate of 1 kHz. Excitation using a low repetition rate but high pulse energies allows to generate large densities of PEPs without the thermal damage associated to high duty-cycle excitation.

ACKNOWLEDGMENT

We sincerely thank Martin Könemann for providing us the organic dye. We are grateful of Marc A. Verschuuren for the fabrication of the samples. This research was financially supported by the Nederlandse Organisatie voor Wetenschappelijk Onderzoek (NWO) through the project LEDMAP of the Technology Foundation STW and through the Industrial Partnership Program Nanophotonics for Solid State Lighting between Philips and the Foundation for Fundamental Research on Matter FOM. This work has been also funded by the European Research Council (ERC-2011-AdG proposal No. 290981), by the European Union Seventh Framework Programme under Grant Agreements FP7-PEOPLE-2013-CIG-630996 and FP7-PEOPLE-2013-CIG-618229, and the Spanish MINECO under Contract No. MAT2014-53432-C5-5-R.

AUTHOR CONTRIBUTIONS

M.R., A.H. and S.R.K.R. designed and performed the experiments and analyzed the data. A.I.F.D. and J.F. performed the calculations and simulations. J.G.R. and F.J.G.V.

supervised the project. All authors discussed the results and commented on the manuscript.

- [1] Weisbuch, C., Nishioka, M., Ishikawa, A. and Arakawa, Y. Observation of the coupled exciton-photon mode splitting in a semiconductor quantum microcavity. *Physical Review Letters* **69**, 3314 (1992).
- [2] Baumberg, J. J., Savvidis, P. G., Stevenson, R. M., Tartakovskii, A. I., Skolnick, M. S., Whittaker, D. M. and Roberts, J. S. Parametric oscillation in a vertical microcavity: A polariton condensate or micro-optical parametric oscillation. *Physical Review B* **62**, R16247 (2000).
- [3] Saba, M., Ciuti, C., Bloch, J., Thierry-Mieg, V. and André, R. High-temperature ultrafast polariton parametric amplification in semiconductor microcavities. *Nature* **414**, 731 (2001).
- [4] Kasprzak, J., Richard, M., Kundermann, S., Baas, A., Jeambrun, P., Keeling, J. M. J., Marchetti, F. M., Szymańska, M. H., André, R., Staehli, J. L., Savona, V., Littlewood, P. B., Deveaud, B. and Dang, L. S. Bose–Einstein condensation of exciton polaritons *Nature* **443**, 409 (2006).
- [5] Amo, A., Lefrère, J., Pigeon, S., Adrados, C., Ciuti, C., Carusotto, I., Houdré, R., and Giacobino, E., and Bramati, A. Superfluidity of polaritons in semiconductor microcavities *Nature Physics* **5**, 805 (2009).
- [6] Lidzey, D. G., Bradley, D.D.C., Skolnick, M. S. and Virgili, T. Strong exciton–photon coupling in an organic semiconductor microcavity *Nature* **395**, 53-55 (1998).
- [7] Bellessa, J., Bonnand, C., Plenet, J. C. and Mugnier, J., T. Strong Coupling between Surface Plasmons and Excitons in an Organic Semiconductor *Physical Review Letters* **93**, 036404 (2004).
- [8] Dintinger, J., Klein, S., Bustos, F., Barnes, W. L. and Ebbesen, T. W. Strong coupling between surface plasmon-polaritons and organic molecules in subwavelength hole arrays. *Physical Review B* **71**, 035424 (2005).
- [9] Kéna-Cohen, S., Davanço, M. and Forrest, S. R. Strong Exciton-Photon Coupling in an Organic Single Crystal Microcavity. *Physical Review Letters* **101**, 116401 (2008).
- [10] Aberra Guebrou, S., Symonds, C., Homeyer, E., Plenet, J. C., Gartstein, N. Y., Agranovich, V. M. and Bellessa, J. Coherent Emission from a Disordered Organic Semiconductor Induced by Strong Coupling with Surface Plasmons. *Physical Review Letters* **108**, 066401 (2012).

- [11] Kéna-Cohen, S. and Forrest, S. R. Room-temperature polariton lasing in an organic single-crystal microcavity. *Nature Photonics* **4**, 371-375 (2010).
- [12] Plumhof, J. D., Stöferle, T., Mai, L., Scherf, U. and Mahrt, R. F. Room-temperature polariton lasing in an organic single-crystal microcavity. *Nature Materials* **13**, 247 (2014).
- [13] Daskalakis, K. S., Maier, S. A., Murray, R. and Kéna-Cohen, S. Nonlinear interactions in an organic polariton condensate. *Nature Materials* **13**, 271-278 (2014).
- [14] Feist, J. and Garcia-Vidal, F. J. Extraordinary Exciton Conductance Induced by Strong Coupling. *Physical Review Letters* **114**, 196402 (2015).
- [15] Schachenmayer, J., Genes, C., Tignone, E. and Pupillo, G. Cavity-Enhanced Transport of Excitons. *Physical Review Letters* **114**, 196403 (2015).
- [16] Orgiu, E., George, J., Hutchison, J. A., Devaux, E., Dayen, J. F., Doudin, B., Stellacci, F., Genet, C., Schachenmayer, J., Genes, C., Pupillo, G., Samori, P., Ebbesen, T. W. Conductivity in organic semiconductors hybridized with the vacuum field. *Nature Materials* **114**, 1123-1129 (2015).
- [17] Spano, F. C. Optical microcavities enhance the exciton coherence length and eliminate vibronic coupling in J-aggregates. *The Journal of Chemical Physics* **142**, 184707 (2015).
- [18] Galego, J., Garcia-Vidal, F. J. and Feist, J. Cavity-Induced Modifications of Molecular Structure in the Strong-Coupling Regime. *Physical Review X* **5**, 041022 (2015).
- [19] Hakala, T. K., Toppari, J. J., Kuzyk, A., Pettersson, M., Tikkanen, H., Kunttu, H. and Törmä, P. Vacuum Rabi Splitting and Strong-Coupling Dynamics for Surface-Plasmon Polaritons and Rhodamine 6G Molecules. *Physical Review Letters* **103**, 053602 (2009).
- [20] Rodriguez, S. R. K. and Gómez-Rivas J. Plasmonic Surface Lattice Resonances at the Strong Coupling Regime. *Optics Express* **21**, 27411 (2013).
- [21] Rodriguez, S. R. K., Feist, J., Verschuuren, M. A., García-Vidal, F. J. and Gómez-Rivas, J. Thermalization and Cooling of Plasmon-Exciton Polaritons: Towards Quantum Condensation. *Physical Review Letters* **111**, 166802 (2013).
- [22] Väkeväinen, A. I., Moerland, R. J., Rekola, H. T., Eskelinen, A. P., Martikainen, J. P., Kim, D. H. and Törmä, P. Plasmonic Surface Lattice Resonances at the Strong Coupling Regime. *Nano letters* **14**, 1721 (2014).
- [23] Eizner, E., Avayu, O., Ditcovski, R., and Ellenbogen, T. Plasmonic Surface Lattice Resonances at the Strong Coupling Regime. *Nano letters* **15**, 6215 (2015).

- [24] Zengin, G., Wersäll, M., Nilsson, S., Antosiewicz, T. J., Käll, M. and Shegai, T. Realizing Strong Light-Matter Interactions between Single-Nanoparticle Plasmons and Molecular Excitons at Ambient Conditions. *Physical Review Letters* **114**, 157401 (2015).
- [25] García de Abajo, F. J. *Colloquium: Light scattering by particle and hole arrays. Reviews of Modern Physics* **79**, 1267 (2007).
- [26] Abass, A., Rodriguez, S. R. K., Gómez-Rivas, J. and Maes, B. Tailoring Dispersion and Eigenfield Profiles of Plasmonic Surface Lattice Resonances. *ACS Photonics* **1**, 61 (2014).
- [27] Zou, S., Janel, N., Schatz, G. C. Silver nanoparticle array structures that produce remarkably narrow plasmon lineshapes. *The Journal of Chemical Physics* **120**, 10871 (2004).
- [28] Guo, K., Lozano, G., Verschuuren, M. A., Gómez-Rivas, J. Silver nanoparticle array structures that produce remarkably narrow plasmon lineshapes. *Journal of Applied Physics* **118**, 073103 (2015).
- [29] Vecchi, G., Giannini, V. and Gómez-Rivas, J. Shaping the Fluorescent Emission by Lattice Resonances in Plasmonic Crystals of Nanoantennas. *Physical Review Letters* **102**, 146807 (2009).
- [30] Humphrey, A. D. and Barnes, W. L., J. Plasmonic surface lattice resonances on arrays of different lattice symmetry. *Physical Review B* **90**, 075404 (2014).
- [31] Oulton, R. F., Sorger, V. J., Zentgraf, T., Ma, R.-M., Gladden, C., Dai, L., Bartal, G. and Zhang, X. Plasmon lasers at deep subwavelength scale. *Nature* **461**, 629 (2009).
- [32] van Beijnum, F., van Veldhoven, P. J., Geluk, E. J., de Dood, M. J. A., 't Hooft, G. W. and van Exter, M. P. Surface Plasmon Lasing Observed in Metal Hole Arrays. *Physical Review Letters* **110**, 206802 (2013).
- [33] Suh, J. Y., Kim, C. H., Zhou, W., Huntington, M. D., Co, D. T., Wasielewski, M. R. and Odom, T. W. Plasmonic Bowtie Nanolaser Arrays. *Nano letters* **12**, 11 (2012).
- [34] Zhou, W., Dridi, M., Suh, J. Y., Kim, C. H., Co, D. T., Wasielewski, M. R., Schatz, G. C. and Odom, T. W. Lasing action in strongly coupled plasmonic nanocavity arrays. *Nature Nanotechnology* **8**, 506-511 (2013).
- [35] Gomez, D. E., Vernon, K. C., Mulvaney P. and Davis T. J. Surface Plasmon Mediated Strong Exciton-Photon Coupling in Semiconductor Nanocrystals. *Nano letters* **10**, 274 (2010).
- [36] Schokker, A. H. and Koenderink, A. F. Lasing at the band edges of plasmonic lattices. *Physical Review B* **90**, 155452 (2014).

- [37] Konemann, M., Bohm A., Pschirer, N. G., Qu J., Mattern G. Substituted Rylene Derivatives. U.S. Patent No. 20080167467 A1(2008).
- [38] Giannini, V., Vecchi, G. and Rivas, J. G., Lighting up multipolar surface plasmon polaritons by collective resonances in arrays of nanoantennas. *Physical Review Letters* **105**, 266801 (2010).
- [39] Evlyukhin, A. B., Reinhardt, C., Zywiets, U. and Chichkov, B. N. Collective resonances in metal nanoparticle arrays with dipole-quadrupole interactions. *Physical Review B* **85**, 245411 (2012). Collective resonances in metal nanoparticle arrays with dipole-quadrupole interactions. *Physical Review B* **85**, 245411 (2012).
- [40] Turnbull, G. A., Andrew, P., Jory, M. J., Barnes, W. L., and Samuel, I. D. W. Relationship between photonic band structure and emission characteristics of a polymer distributed feedback laser. *Physical Review B* **64**, 125122 (2001).
- [41] Palik, E. D. Handbook of Optical Constants of Solids (Academic Press, San Diego 1985).
- [42] Lakowicz, J. R., Principles of Fluorescence Spectroscopy (Springer, New York, 2006).
- [43] Imamoglu, A., Ram, R. J., Pau, S., Yamamoto, Y. Collective resonances in metal nanoparticle arrays with dipole-quadrupole interactions. *Physical Review A* **53**, 4250 (1996).
- [44] Mazza, L., Fontanesi, L. and La Rocca, G. C. Organic-based microcavities with vibronic progressions: Photoluminescence. *Physical Review B* **80**, 235314 (2009).
- [45] Mazza, L., Kéna-Cohen, S., Michetti, P. and La Rocca, G. C. Microscopic theory of polariton lasing via vibronically assisted scattering. *Physical Review B* **88**, 075321 (2013).
- [46] Ówik, J. A., Reja, S., Littlewood, P. B. and Keeling, J. Polariton condensation with saturable molecules dressed by vibrational modes. *EPL (Europhysics Letters)* **105**, 47009 (2014).
- [47] Somaschi, N., Mouchliadis, L., Coles, D., Perakis, I. E., Lidzey, D. G., Lagoudakis, P. G. Savvidis, P. G. Ultrafast polariton population build-up mediated by molecular phonons in organic microcavities. *Applied Physics Letters* **99**, 143303 (2011).
- [48] Ji, R., Hornung, M., Verschuuren, M. A., van de Laar R., van Eekelen J., Plachetka U., Moeller M. and Moormann C. UV enhanced substrate conformal imprint lithography (UV-SCIL) technique for photonic crystals patterning in LED manufacturing, *Microelectronic Engineering* **87**, 963-967 (2010).

I. SUPPLEMENTARY INFORMATION: PLASMON-EXCITON-POLARITON LASING

A. Electromagnetic calculations modelling SLRs and extinction measurements

In order to gain insight in the distribution of the electric field supported by the array of silver nanoparticles, we have performed finite-difference time domain (FDTD, LumericalTM) and Finite Element Method (FEM, Comsol MultiphysicsTM) simulations on the nanoparticle array covered by 260 nm layer of PMMA. In Fig. S1 (a,c), the extinction measurements for incident polarizations along the short and long axis of the nanoparticles are shown. In both panels, the extinction of the array is plotted as a function of optical frequency (energy) and the angle of incidence, θ_{in} , which is related to the in-plane wave-vector by $k_{||} = \frac{2\pi}{\lambda} \sin(\theta_{in})$. Fig. S1 (b,d) renders FDTD simulations for these two experimental maps, showing an excellent agreement between experimental and numerical results. FEM calculations were performed on the same system, and are not shown here because of their exact correspondence with FDTD results.

FDTD and FEM calculations were performed within a unit-cell describing a perfectly periodic rectangular array. Bloch boundary conditions were set at the edges of the unit-cell along the in-plane (xy) directions, and perfect matched layers (PML) were applied along the out-of-plane (z) direction. The upper surface of the silver particles is generally oxidized, reducing the size of the particle. From high-resolution SEM images we have estimated that in our samples a 15 nm oxide is formed on each side of the particle. This oxidation occurs despite the fact that the array is covered by 20 nm Si_3N_4 and 10 nm SiO_2 protection layers. The permittivity for the different materials in the samples were modeled through fits to experimental data taken from previous literature[1]. In the FDTD simulations, an override mesh with the finesse of 1 nm was used in the regions occupied by the silver nanoparticles. In the FEM calculations, conformal meshing of similar dimensions was employed to accommodate the spatial discretization of Maxwell's Equations to the particles shape.

The maps for incident beam polarization parallel to the short axis of the particles (Fig. S1(a,b)) show an extinction band at energies larger than 2.5 eV. This band corresponds to a dipolar like localized surface plasmon resonance ($\lambda/2$ -resonance) oriented along the short axis. The dispersive extinction band around 2.1 eV is caused by the SLR that arises from

the radiative coupling between $\lambda/2$ -resonances supported by neighboring particles, which is mediated by the $(0, \pm 1)$ Rayleigh anomalies (RAs). RAs correspond to the in-plane diffraction orders for the particle array [2–4]. Therefore, their dispersion is determined by the conservation of the in-plane wave-vector,

$$\pm \vec{k}_{\parallel d} = \vec{k}_{\parallel i} \pm \vec{G}, \quad (2)$$

where $\vec{k}_{\parallel d} = \frac{2\pi}{\lambda} n_{eff} \hat{u}_d$ and $\vec{k}_{\parallel i} = \frac{2\pi}{\lambda} \sin(\theta) \hat{u}_i$ are the parallel components of the diffracted and incident wave-vectors, respectively (\hat{u}_d and \hat{u}_i are the unitary vectors along the diffracted and incident directions), \vec{G} is the reciprocal lattice vector of the array, θ is the angle between the wave-vector of the incident beam and the direction normal to the sample, and n_{eff} is the effective index defining the phase velocity of the in-plane diffracted wave. The extinction band in the maps for incident polarization parallel to the long axis of the particles show a well defined extinction band at 2.35 eV (Fig. S1(c,d)). This band originates from the quadrupolar-like ($3\lambda/2$) resonance that the nanoparticles support along this direction [5]. The dispersive band at lower energies is due to the SLR arising from the radiative coupling of the $3\lambda/2$ -resonances through the $(0, \pm 1)$ RAs.

Electric field amplitude maps obtained through FEM simulations are shown in the main text. Similarly, Fig. S2 shows FDTD electric field intensity distributions (long axis polarization) within the xy -plane at half the height of the nanoparticles. Panel (a) is evaluated for an incident plane wave with $\theta_{in} = 1.5^\circ$ and 2.13 eV, whereas panel (b) corresponds to 24° and 2.26 eV. Both configurations match SLR dispersion in the extinction maps. At angles close to normal incidence, a quadrupolar-like field distribution can be observed. The underlying $3\lambda/2$ -resonance gives rise to a reduction in the far-field scattered power. Consequently, the SLR is very narrow, and the array extinction is low due to the suppression of radiation losses. By increasing the angle of incidence, the $(0, \pm 1)$ SLR band becomes brighter and broader (Fig. S2 (c,d)). This behavior can be explained through the electric field profile in Fig. S2(b). It shows that the field distribution at oblique angles resembles more a dipolar resonance, which is caused by the retardation introduced by diffractive scattering within the array plane.

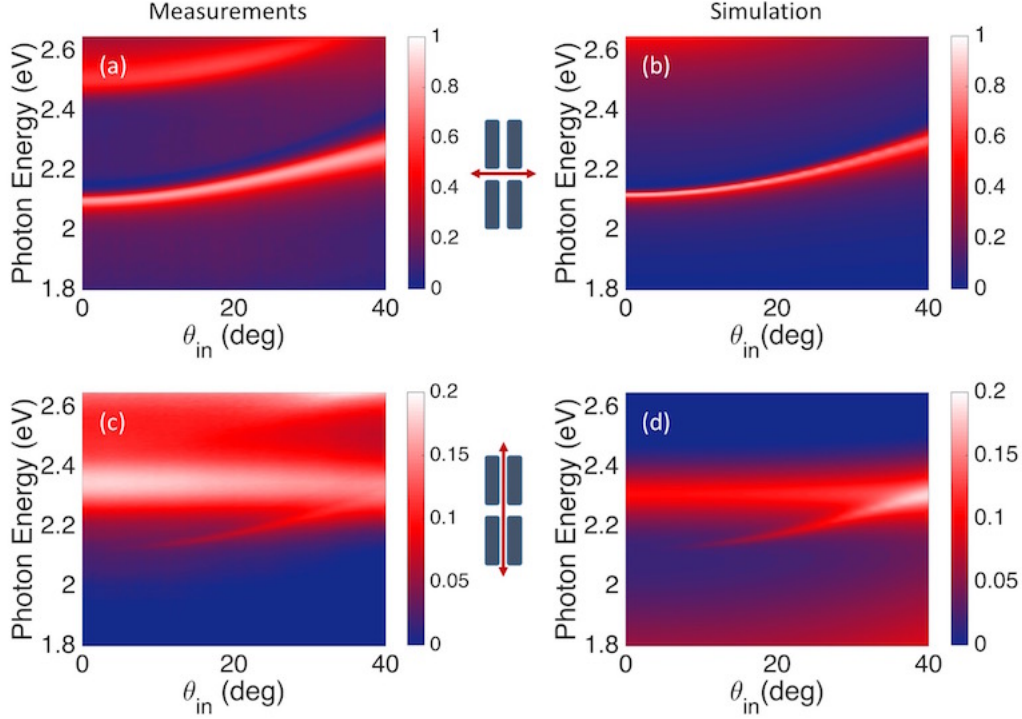


FIG. S1. Angle-resolved measurements (a) and FDTD simulation (b) of the extinction by an array of silver nanoparticles illuminated by a plane wave polarized along the short axis of the nanoparticles. (c,d) are the experimental and simulated angle-resolved extinction for the incident light polarized along the long axis of the nanoparticles.

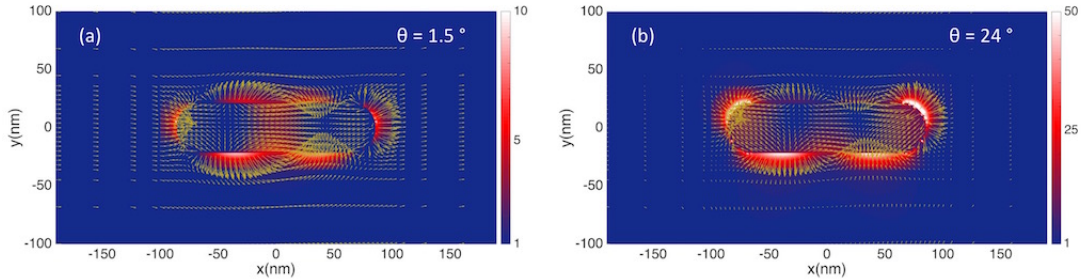


FIG. S2. FDTD electric field intensity within the xy -plane at half the height of the particles for an incident plane wave at an angle of (a) 1.5° and (b) 24° (Note the different scales in both panels). The polarization of the incident wave is parallel to the nanoparticles long axis. The arrows correspond to the real component of the in-plane electric field.

B. Lifetime and quantum efficiency

It is well known that increasing dye concentration enhances intermolecular interactions. These interactions are usually detrimental for emission purposes, as it leads to spontaneous aggregation (modification of the spectral properties of the sample), and to a reduction of fluorescence lifetime (τ) due to the enhancement of non-radiative decay channels (concentration quenching of the emission). To quantify the concentration quenching, we have prepared several layers of PMMA with different concentrations of dye molecules and measured τ using time-correlated single photon counting (See Fig. S3(a)). To excite the samples, a pulse diode laser with repetition rate of 40 MHz and excitation wavelength of 375 nm (3.3 eV) is used. We also estimate the quantum efficiency (QE) of the layers with various concentrations (See Fig. S3(b)). For the quantum yield measurements, a home-built integrating sphere with continuous-wave excitation at a wavelength of 532 nm (2.33 eV) is used. At $C = 5 \text{ wt}\%$, $\tau = 5.5 \text{ ns}$ and the associated QE is 72%, consistent with typical values for laser dyes. By increasing the concentration of dye molecules to $C = 35 \text{ wt}\%$, τ is reduced to 0.5 ns and QE drops to 3.5 %. It should be noted, that the relative strength of the bands in the emission and absorption spectra are not modified by increasing concentration, suggesting that there is no formation of new dimeric or oligomeric species, as it can be the case for xanthene dyes. Therefore, we conclude that the dye molecules in our samples do not suffer significant aggregation effects at high concentrations.

C. Extinction measurements for different dye concentration

Extinction measurements on the arrays of plasmonic nanoparticles covered with 260 nm PMMA doped with different dye concentrations are shown in Fig. S4. In the top (bottom) row, the polarization of the incident beam is along the short (long) axis so that bright (dark) SLRs can be probed (See Fig. S1). At $C = 0 \text{ wt}\%$, uncoupled modes are illustrated. By increasing the concentration to $C = 15 \text{ wt}\%$ the onset of hybridization between the excitons and SLRs becomes apparent. The coupling between molecular excitons and SLRs strengthens by increasing the concentration to 25 wt% and 35 wt%, while the associated Rabi splittings becomes wider.

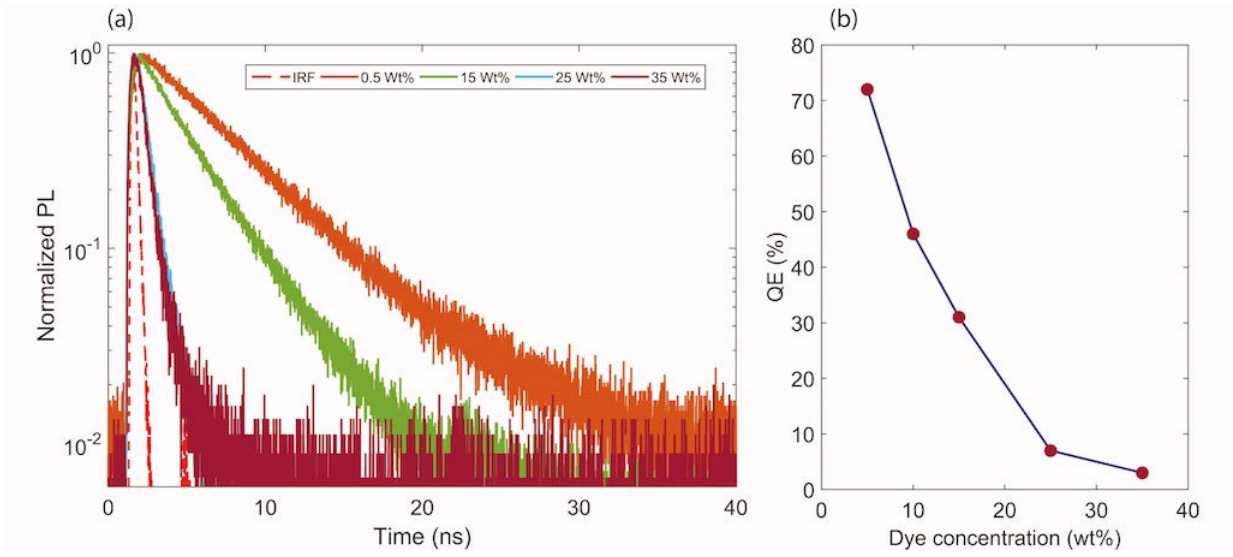


FIG. S3. (a) Fluorescence lifetime measurements for the PMMA layers with different dye concentrations. (b) Quantum efficiency of the dye doped layer for different concentrations.

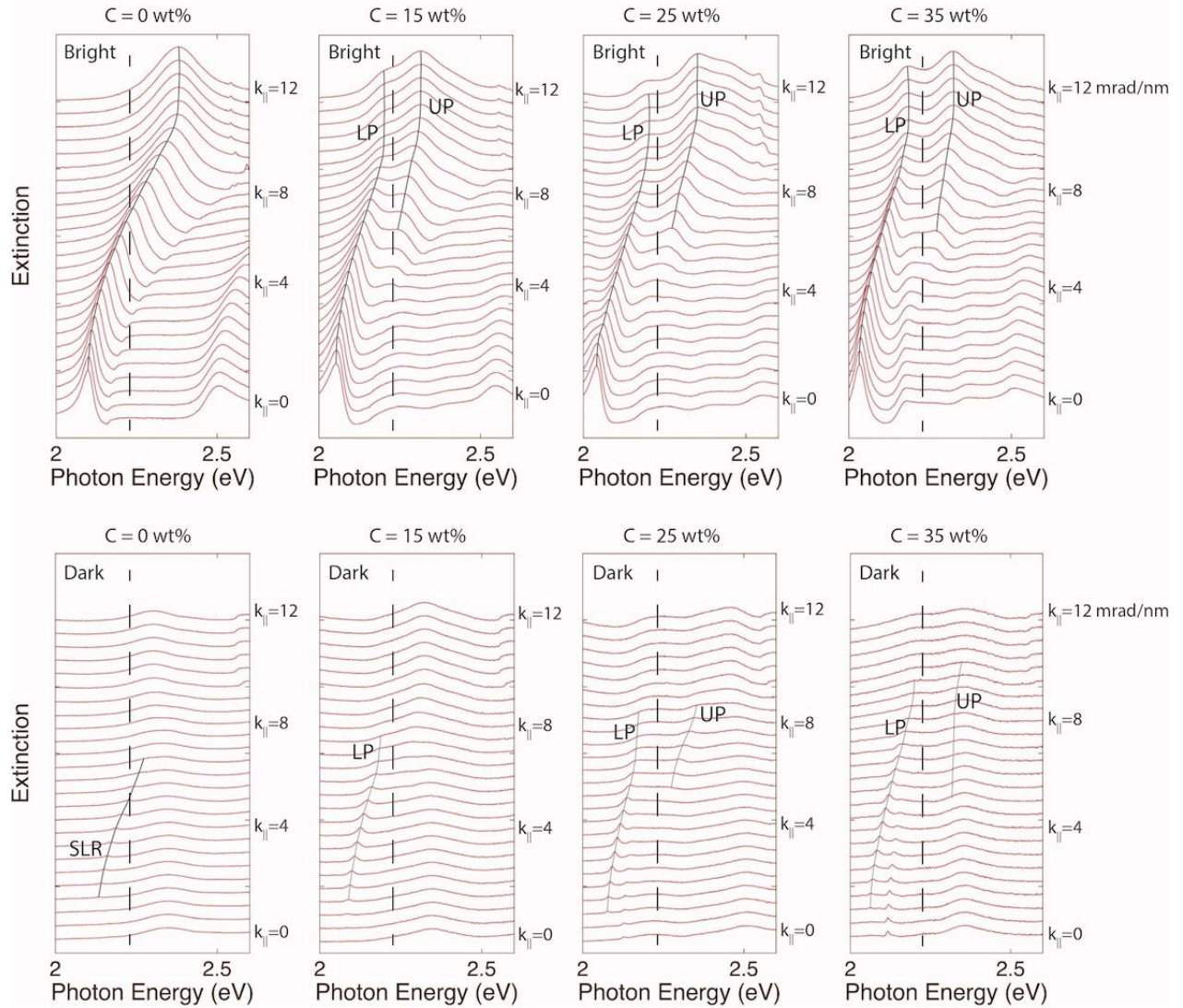


FIG. S4. Extinction measurements for different $k_{||}$ of the samples with various dye concentrations for polarization perpendicular (top row) and parallel (bottom row) to the long axis of the nanoparticles. The energy of the molecular excitonic transition at 2.24 is shown by the dashed line in each panel.

-
- [1] Palik, E. D. Handbook of Optical Constants of Solids (Academic Press, San Diego 1985).
 - [2] Zou, S., Janel, N., Schatz, G. C. Silver nanoparticle array structures that produce remarkably narrow plasmon lineshapes. *The Journal of Chemical Physics* **120**, 10871 (2004).
 - [3] Kravets, V. G., Schedin, F. and Grigorenko, A. N. Extremely Narrow Plasmon Resonances Based on Diffraction Coupling of Localized Plasmons in Arrays of Metallic Nanoparticles. *Phys-*

ical Review Letters **101**, 087403 (2008).

- [4] Humphrey, A. D. and Barnes, W. L., J. Plasmonic surface lattice resonances on arrays of different lattice symmetry. *Physical Review B* **90**, 075404 (2014).
- [5] Giannini, V., Vecchi, G. and Rivas, J. G., Lighting up multipolar surface plasmon polaritons by collective resonances in arrays of nanoantennas. *Physical Review Letters* **105**, 266801 (2010).